NANO LETTERS

LETTER

pubs.acs.org/NanoLett

Room Temperature Current Injection Polariton Light Emitting Diode with a Hybrid Microcavity

Tien-Chang Lu,[*,†] Jun-Rong Chen,[†] Shiang-Chi Lin,[†] Si-Wei Huang,[†] Shing-Chung Wang,[*,†] and Yoshihisa Yamamoto[‡,§]

[†]Department of Photonics, National Chiao Tung University, Hsinchu 300, Taiwan

[‡]E. L. Ginzton Laboratory, Stanford University, Stanford California 94305, United States

[§]National Institute of Informatics, Hitotsubashi, Chiyoda-ku, Tokyo 101-8430, Japan

ABSTRACT: The strong light−matter interaction within a semiconductor high-Q microcavity has been used to produce half-matter/half-light quasiparticles, exciton-polaritons. The exciton-polaritons have very small effective mass and controllable energy-momentum dispersion relation. These unique properties of polaritons provide the possibility to investigate the fundamental physics including solid-state cavity quantum electrodynamics, and dynamical Bose−Einstein condensates (BECs). Thus far the polariton BEC has been demonstrated using optical excitation. However, from a practical viewpoint, the current injection polariton devices operating at room temperature would be most desirable. Here we report the first realization of a current injection microcavity GaN exciton-polariton light emitting diode (LED) operating under room temperature. The exciton-polariton emission from the LED at photon energy 3.02 eV under strong coupling condition is confirmed through temperature-dependent and angle-resolved electroluminescence spectra.

KEYWORDS: GaN, exciton-polariton, light emitting diode (LED), Rabi splitting

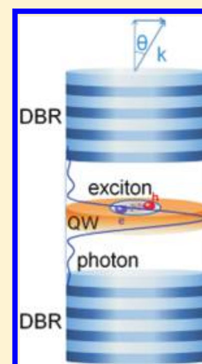

Strong light-matter interactions in semiconductor high-Q microcavities have attracted much attention over the past twenty years due to their potential to probe fundamental physics and create practical devices. Exciton-polaritons are bosonic particles with very small effective mass (typically 10^{-4} times the bare exciton mass) and controllable energy-momentum dispersion curves by appropriate detuning.[1] These unique properties have led to demonstration of a wealth of experimental results, including cavity quantum electrodynamics,[2] dynamical Bose−Einstein condensates (BEC) or polariton lasers,[3−9] and polariton parametric amplifiers.[10] Thus far the polariton BEC or lasing has been demonstrated in GaAs,[5,6] CdTe,[3] organic materials,[7] and GaN.[8,9] Nevertheless, these results are mostly based on optical pumping and low-temperature experiments. Toward a polariton optoelectronic device for practical applications, electrically pumped exciton-polariton emitters operating at room-temperature would be an important step toward that goal.

An electrically pumped microcavity light-emitting diode (LED) has been demonstrated for organic semiconductors.[11] A mid-infrared polariton LED based on a GaAs/AlGaAs quantum cascade structure has been reported.[12] More recently, electrically pumped GaAs semiconductor polariton LEDs have been demonstrated at temperature from 10 to 315 K.[13−16] However, no current injection wide bandgap semiconductor polariton LED has been reported yet. A GaN microcavity exciton-polariton LED possesses several unique advantages over other material systems. First, GaN has a small Bohr radius and large exciton binding energy (40 meV for quantum well), so that exciton-polaritons can exist at high temperatures.[17,18] Second, a GaN exciton has a fast phonon-assisted relaxation rate, which can effectively suppress the relaxation bottleneck and achieve the efficient thermalization.[19] Third, a GaN exciton has a large oscillator strength that leads to significant increase in the Rabi splitting and Rabi oscillation frequency.[20] Besides, in the exciton-polariton LED, the inhomogeneous broadening due to exciton localization and the nonradiative decay can be suppressed by the strong coupling between cavity photons and localized excitons. This is an important advantage for a highly inhomogeneous material system such as GaN. Nevertheless, for realization of an electrically pumped GaN-based polariton LED, there are several technical difficulties including the growth of high-reflectivity nitride-based distributed Bragg reflectors (DBRs), high-conductivity p-type GaN material, and high-quality GaN-based quantum wells (QWs).[21]

In this paper, we report the first realization of an electrically pumped GaN-based exciton-polariton LED in a microcavity with carefully designed nanostructures within the microcavity to achieve high optical quality and high cavity reflectivity. The GaN-based microcavity, shown schematically in Figure 1a, consists of a 29-pair AlN/GaN bottom DBR and a 5λ-thick optical cavity layer composed of an n-type GaN, 10 $In_{0.15}Ga_{0.85}N$/GaN multiple quantum wells (MQWs) at an antinode position, and a p-type GaN layer. The thicknesses of quantum well and barrier are 2 and 8 nm, respectively. The grown 29-pair AlN/GaN bottom DBR showed a reflectivity of $R = 99.4\%$ with a spectral bandwidth of ~25 nm. In order to reduce the tensile strain between the AlN and GaN to achieve high optical quality and high reflectivity DBR, we inserted one superlattice (SL) into each five DBR periods at first twenty pairs of bottom DBR. Then the superlattice was inserted into each three DBR periods for the

Received: April 4, 2011
Revised: June 9, 2011
Published: June 15, 2011

ACS Publications © 2011 American Chemical Society

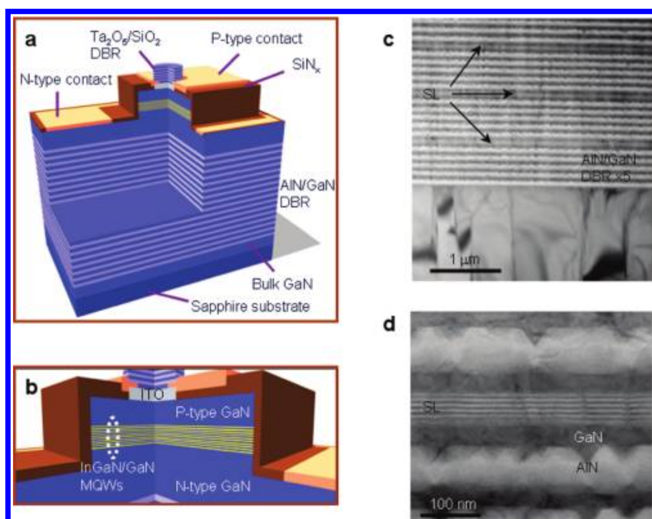

Figure 1. Schematic sketch of the electrically pumped InGaN-based polariton LED. (a) The GaN-based hybrid microcavity consists of a 29-pair AlN/GaN bottom DBR and a 5λ optical thickness microcavity composed of a n-type GaN, 10 pairs $In_{0.15}Ga_{0.85}N$/GaN MQWs, a p-type GaN layer, an ITO layer and an 8-pair Ta_2O_5/SiO_2 top DBR. (b) An enlarged active region including an ITO layer, MQWs, and p- and n-type GaN layers. (c) Cross-sectional TEM image of the superlattice DBR structure. (d) Cross-sectional TEM image of one set of 5.5-pairs AlN/GaN SL insertion layers under high magnification.

remaining nine pairs of bottom DBR.[22] The thicknesses of AlN and GaN layers are about 5 and 2.8 nm, respectively, in the SL structure and the total thickness of SL have to be grown carefully to match the phase of DBR design. The epitaxially grown structure was then processed to form the intracavity coplanar p- and n-contacts for current injection. A 0.2 μm thick SiN$_x$ layer was used as the mask to form a current injection and light emitting aperture of 30 μm in diameter. A 30 nm thick indium−tin-oxide (ITO) layer was then deposited on the current aperture to serve as the transparent contact layer (Figure 1b). The ITO was annealed at 525 °C under the nitrogen ambient to reduce the contact resistance as well as to increase transparency thus reducing the internal cavity loss. After that, the metal contact layer was deposited by the electron beam evaporation using Ti/Al/Ni/Au (20/150/20/1000 nm) and Ni/Au (20/1000 nm) as the n-type electrode and p-type electrode to form coplanar intracavity contacts, respectively. Finally an 8-pair Ta_2O_5/SiO_2 dielectric top DBR with a reflectivity of R = 99% was deposited to achieve a reasonable quality factor (Q-factor ≅ 400). The cross-sectional transmission electronic microscopy (TEM) image of the SL DBR structure is shown in Figure 1c. The lighter layers represent AlN layers while the darker layers represent GaN layers. The interfaces between AlN and GaN layers are sharp and abrupt in the low-magnification TEM image. Figure 1d shows the cross-sectional TEM image of one set of 5.5-pairs AlN/GaN SL insertion layers under high magnification. V-shaped surfaces observed on top of AlN layers were formed in order to partially release the crystal stress because the thickness of AlN layer in DBRs has been larger than the critical thickness. However, the residual tensile stress in DBRs accumulates alone with the DBR thickness. Here, the nanoscale AlN/GaN SL layers play an important role for the reduction of remaining in-plane tensile stress and being responsible for the crack suppression and improvement in the reflectivity of the DBRs.

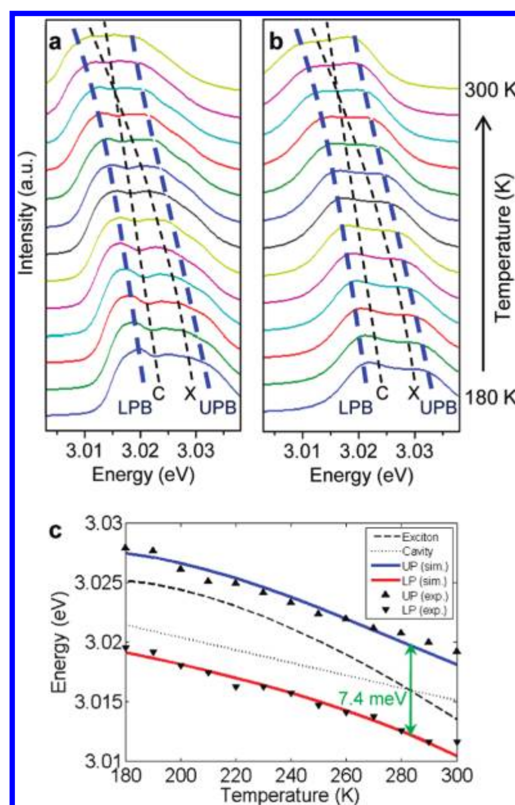

Figure 2. Polariton electroluminescence emission as a function of temperatures. (a) Experimentally measured temperature-dependent electroluminescence spectra from 180 to 300 K when the input current is 2 mA. (b) Theoretically calculated temperature-dependent transmission spectra from 180 to 300 K. The detuning between exciton mode (X) and cavity photon mode (C) changes with increasing temperature. The spectra shown in (a,b) are normalized for easily identifying the emission peaks. Both results show the characteristic anticrossing behavior. Rabi splitting of 7.4 meV is observed at 280 K. (c) Extracted peaks of the polariton emission shown in (a) by Gaussian fitting and simulated energy curves of uncoupled exciton and photon modes and lower and upper polariton modes.

Two commonly used experimental techniques are employed to confirm the strong coupling and the anticrossing behavior of the QW excitons and cavity photons in the fabricated InGaN/GaN microcavity device. One is the temperature-dependent electroluminescence and the other is angle-resolved electroluminescence.[23,24] The former technique mainly relies on the temperature-dependent variation of bandgap energy to tune the QW exciton energy crossing the cavity photon energy. The latter technique uses the parabolic dispersion with increasing emission angle to adjust the detuning parameter between the cavity photon and the QW exciton. The angle-resolved electroluminescence measurement can prevent collective coupling of a set of cavity modes and ensure the exciton only couple to one cavity mode. The temperature-dependent measurements are performed in a temperature-controlled, closed-cycle, liquid nitrogen cryostat, and the angle-resolved measurements were carried out by using a 600 μm core UV optical fiber mounted on a rotating arm. The angular resolution is about 1° and the emission is detected by a liquid nitrogen cooled charge-coupled device (CCD) attached to a 320 mm single monochromator with a spectral resolution of about 0.2 nm.

Figure 2a shows experimental electroluminescence spectra from the GaN-based microcavity for different temperatures

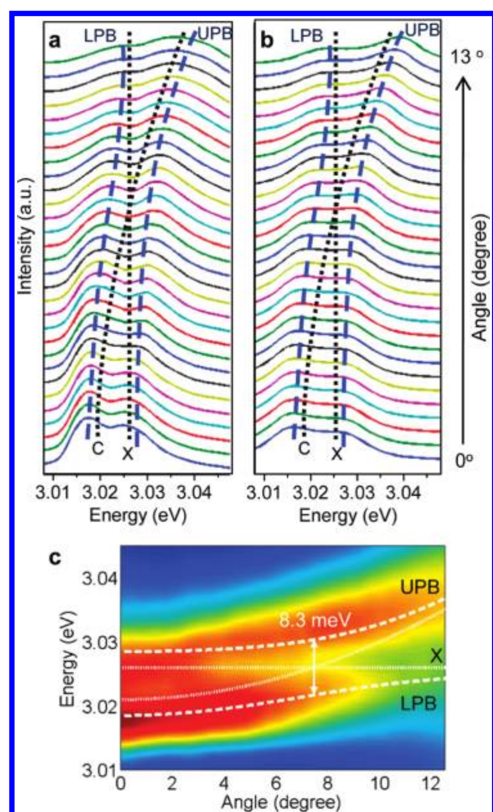

Figure 3. Angle-resolved polariton electroluminescence spectra. (a) Experimentally measured angle-resolved electroluminescence spectra from 0 to 13° when the input current is 2 mA at 180 K. (b) Theoretically calculated angle-resolved transmission spectra from 0 to 13°. The detuning between exciton mode (X) and cavity photon mode (C) changes with increasing angle both results show the characteristic anticrossing behavior. The spectra shown in (a,b) are normalized for easily identifying the emission peaks. (c) Color map of the measured polariton angular dispersion. The horizontal dotted lines are the bare exciton mode and the curve dotted lines are the cavity mode. Rabi splitting of 8.3 meV is observed at 7.4°.

between 180 and 300 K at a collection angle of zero degree and at the input current of 2 mA. The emission spectrum at 180 K exhibits two peaks of exciton-like upper polariton branch (UPB) and photon-like lower polariton branch (LPB). This condition is commonly termed as negative detuning. With increasing the temperature, the decrease in the QW exciton energy resulted from a reduction of the bandgap energy, overwhelms the decrease in the cavity photon energy due to the temperature dependence of the refractive index. Since the QW exciton energy is much more significantly affected by the temperature change than the cavity photon energy, the detuning will be changed from negative to positive detuning with increasing temperature from 180 to 300 K. An anticrossing dispersion is clearly exhibited, which confirms that the cavity system is in a strong coupling regime even at 300 K. To understand the temperature-dependent electroluminescence spectra obtained from the experiment, we employed the transfer matrix method coupled with a Lorentz oscillator model to calculate the transmission spectra of the microcavity structure. The shift of the cavity photon energy with increasing temperature is estimated to be ~0.054 meV/K[25] and the temperature-dependent QW excitons energy follows the modified Varshni formula including the localization effect $E(T)=E_m(0) - [(\alpha T^2)/(T+\beta)] - [(\sigma^2)/(k_B T)]$, where $E(T)$ is the emission energy at T, $E_m(0)$ is the energy gap at 0 K, α and β are Varshni's fitting parameters, k_B is the Boltzmann constant, and σ is related with localization effect.[26] In this numerical simulation, we use $\alpha \cong 0.435$ meV/K, $\beta \cong 900$ K, and $\sigma \cong 17.5$ meV. These values are estimated from the independent measurements of our bare InGaN/GaN MQWs and are close to the values reported in recent literatures.[26,27] The QW exciton was modeled by a coupled harmonic oscillator dispersive dielectric function, taking into accounts the homogeneous and inhomogeneous broadening line width.[28,29] The simulation results of temperature-dependent spectra from 180 to 300 K are shown in Figure 2b. It is noteworthy that the almost identical evolution of the polariton emission spectra as the experimental spectra is obtained from the numerical simulation by using the exciton damping rate of 7 meV and the inhomogeneous broadening line width of 8 meV for the InGaN QW excitons.[29,30] The emission intensity at 180 K is dominated by photon-like LPB. With increasing temperature, cavity mode couples with exciton mode and shares identical polariton emission at resonance. The estimated oscillator strength of the InGaN/GaN QW exciton is 0.0289 eV^2 per well. This value is of the same order of magnitude as that of bulk GaN (0.03−0.04 eV^2) and GaN/AlGaN QW (0.05 eV^2) excitons.[31,32] The relatively smaller oscillator strength value extracted in our data compared that of the bulk GaN could mainly be due to the well-known strong built-in piezoelectric field in the InGaN QW grown on the c-plane that could offset the quantum confinement of the InGaN QW. In addition, the actual device structure and crystal quality of QWs could be the contributing factors in our relatively small value of the oscillator strength. The simulation results reveal that the condition of zero exciton-photon detuning at zero angle is reached at a temperature of 280 K and the normal mode splitting at zero detuning is about 7.4 meV as shown in Figure 2c.

Angle-resolved electroluminescence measurements were performed at 180 K with the input current of 2 mA corresponding to the negative detuning at normal incidence angle for probing the anticrossing behavior as a function of angle. Figure 3a shows the measured angle-resolved electroluminescence spectra, which reveals the well-resolved upper and lower polariton modes and exhibits the anticrossing behavior of the strong coupling regime. A zero detuning is realized at 7.4° and the corresponding normal mode splitting is about 8.3 meV, which is very close to that obtained from the temperature-dependent experiment at 280 K. The calculated angle-resolved spectra (Figure 3b) are in good agreement with the measured results (Figure 3a). To get better understanding of the dispersive features of the two polariton branches, the color maps of the angular dispersion of measured spectra from 0 to 13° are shown in Figure 3c. At small angle (negative detuning), the photon-like LPB shows relatively higher emission intensity since the cavity mode always dominates the emission in a microcavity. As the cavity mode crossing the exciton mode, the high energy line has transformed into photon-like UPB and the intensity emitted from the exciton-like LPB vanishes gradually with increasing angle. This evolution of polariton emission intensity with angle and temperature supports the characteristics of strong coupling. The data from the two measurement techniques agree well each other indicating the strong coupling survive in our device at room temperatures. The relatively small normal mode splitting compared with the previously reported values[18] by optical pumping experiment could originate from the longer cavity length, smaller number of

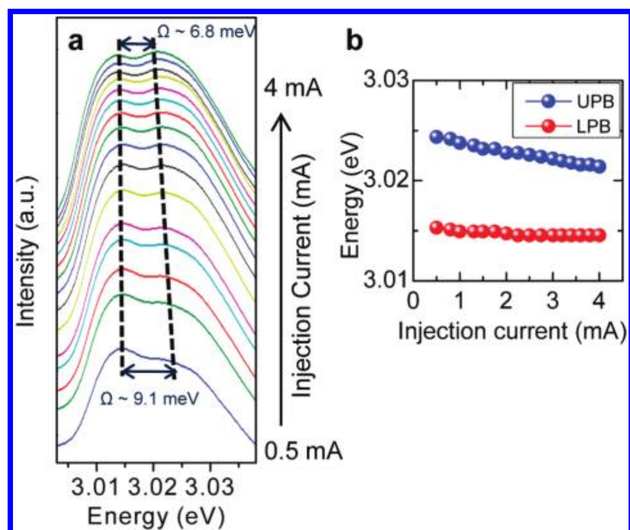

Figure 4. Current-dependent polariton electroluminescence spectra. (a) The normalized polariton electroluminescence spectra as a function of injection current from 0.5 to 4 mA at 240 K. At low injection currents, two clearly resolved polariton peaks are evident. With increasing injection current, the two polariton peaks are progressively close to each other, leading to the decrease in Rabi splitting from 9.1 to 6.8 meV. (b) Extracted lower and upper polariton peak energies by Gaussian fitting of (a), showing the decrease of Rabi splitting with increasing input current.

MQWs or weak optical field overlap with MQWs, and smaller oscillator strength due to the built-in piezoelectric field in the QWs.

We further measured the current-dependent electroluminescence spectra at zero degree of the angle and under the temperature of 240 K when the detuning was closed to the zero. Figure 4a shows the electroluminescence spectra as a function of injection current from 0.5 to 4 mA. At low injection currents, two clearly resolved polariton peaks separated by 9.1 meV are observed. With increasing injection current, the two polariton peaks are progressively close to each other, leading to the decrease in normal mode splitting from 9.1 to 6.8 meV. To estimate the carrier density, we assume that all injected carriers are trapped into the quantum wells, and thus $n = j\tau/e$ where e is the electron charge, j is the current density, and τ is the average carrier lifetime. For 4 mA injection current, the estimated polariton density is $n \sim 1.87 \times 10^{12}$ cm^{-2} if we assume τ = 0.53 ns.[33] This value is much lower than the Mott density in InGaN/GaN QWs ($\sim 1 \times 10^{13}$ cm^{-2}).[33] Figure 4b presents the decrease of Rabi splitting as a function of injection current, which could originate from the increase of homogeneous broadening due to the enhanced exciton−exciton scattering. The apparent red shift trend should be noted as the current stems from the device heating under CW current injection. Additional measurement was performed by a pulsed current source to reduce heating effects. Nevertheless, the decrease in Rabi splitting can also be found as the injection current increased, indicating that the effect of exciton−exciton scattering should dominate the bleaching mechanism of strong coupling. The further increase in injection current was not conducted due to the device heat dissipation problem that could cause some damage to the device. Within our current injection range, we observed that the integrated electroluminescence intensities for both UPB and LPB as functions of injection current show a linear increase trend, which could be due to the strong coupling between cavity photons and excitons in a fast Rabi oscillation that suppresses the nonradiative decay.[15,16]

In conclusion, we have demonstrated an electrically pumped InGaN-based exciton-polariton LED operating at room temperature. Both temperature-dependent electroluminescence spectra and angle-resolved electroluminescence spectra show the existence of anticrossing in the strong coupling regime. Further optimization of device design, including the decrease in ITO thickness, the optimization of ITO annealing condition, the increase in QW number, and the decrease in cavity length, would enhance the device performance. In addition, the improvement of heat dissipation should allow higher injection current operation and possible achievement of a room-temperature electrically pumped polariton laser. Our demonstration of an electrically pumped GaN-based polariton LED at room temperature could open a new way for the realization of high efficient polariton LEDs in the VU region of the spectrum, since polariton LEDs operating in the strong coupling regime could substantially suppress the nonradiative decay. In addition, the significantly lower density of states of polaritons makes extra low-threshold polariton lasers possible as compared to conventional semiconductor lasers based on GaN materials.[20,34]

AUTHOR INFORMATION

Corresponding Author

*E-mail: (T.-C.L.) timtclu@mail.nctu.edu.tw; (S.-C.W.) scwang@mail.nctu.edu.tw.

ACKNOWLEDGMENT

This work has been supported in part by the MOE ATU program and in part by the National Science Council of Taiwan under Contracts NSC99-2221-E-009-035-MY3, NSC99-2120-M-009-007, and NSC98-2923-E-009-001-MY3. J.R.C., S.C.L. and S.W.H. acknowledge C. K. Chen, S. W. Chen, Z. Y. Li, and Professor H. C. Kuo of National Chiao Tung University for sample preparation at an early stage. Y.Y. acknowledges the support from the FIQST-Quantum Information Processing program.

REFERENCES

(1) Weisbuch, C.; Nishioka, M.; Ishikawa, A.; Arakawa, Y. *Phys. Rev. Lett.* **1992**, *69*, 3314–3317.
(2) Vahala, K. J. *Nature* **2003**, *424*, 839–846.
(3) Kasprzak, J.; Richard, M.; Kundermann, S.; Baas, A.; Jeambrun, P.; Keeling, J. M. J.; Marchetti, F. M.; Szymańska, M. H.; André, R.; Staehli, J. L.; Savona, V.; Littlewood, P. B.; Deveaud, B.; Dang, L. S. *Nature* **2006**, *443*, 409–414.
(4) Deng, H.; Weihs, G.; Santori, C.; Bloch, J.; Yamamoto, Y. *Science* **2002**, *298*, 199–202.
(5) Deng, H.; Weihs, G.; Snoke, D.; Bloch, J.; Yamamoto, Y. *Proc. Nat. Acad. Sci. U.S.A.* **2003**, *100*, 15318–15323.
(6) Balili, R.; Hartwell, V.; Snoke, D.; Pfeiffer, L.; West, K. *Science* **2007**, *316*, 1007–1010.
(7) Kéna-Cohen, S.; Forrest, S. R. *Nat Photonics* **2010**, *4*, 371–375.
(8) Christopoulos, S.; Von Högersthal, G. B. H.; Grundy, A. J. D.; Lagoudakis, P. G.; Kavokin, A. V.; Baumberg, J. J.; Christmann, G.; Butté, R.; Feltin, E.; Carlin, J.-F.; Grandjean, N. *Phys. Rev. Lett.* **2007**, *98*, 126405.
(9) Christmann, G.; Butté, R.; Feltin, E.; Carlin, J.-F.; Grandjean, N. *App. Phys. Lett.* **2008**, *93*, 051102.

(10) Saba, M.; Ciuti, C.; Bloch, J.; Thierry-Mieg, V.; André, R.; Dang, L. S.; Kundermann, S.; Mura, A.; Bongiovanni, G.; Staehli, J. L.; Beveaud, B. *Nature* **2001**, *414*, 731–735.
(11) Tischler, J. R.; Bradley, M. S.; Bulović, V.; Song, J. H.; Nurmikko, A. *Phys. Rev. Lett.* **2005**, *95*, 036401.
(12) Sapienza, L.; Vasanelli, A.; Colombelli, R.; Ciuti, C.; Chassagneux, Y.; Manquest, C.; Gennser, U.; Sirtori, C. *Phys. Rev. Lett.* **2008**, *100*, 136806.
(13) Tsintzos, S. I.; Pelekanos, N. T.; Konstantinidis, G.; Hatzopoulos, Z.; Savvidis, P. G. *Nature* **2008**, *453*, 372–375.
(14) Tsintzos, S. I.; Savvidis, P. G.; Deligeorgis, G.; Hatzopoulos, Z.; Pelekanos, N. T. *App. Phys. Lett.* **2009**, *94*, 071109.
(15) Khalifa, A. A.; Love, A. P. D.; Krizhanovskii, D. N.; Skolnick, M. S.; Roberts, J. S. *App. Phys. Lett.* **2008**, *92*, 061107.
(16) Bajoni, D.; Semenova, E.; Lemaître, A.; Bouchoule, S.; Wertz, E.; Senellart, P.; Bloch, J. *Phys. Rev. B* **2008**, *77*, 113303.
(17) Kornitzer, K.; Ebner, T.; Thonke, K.; Sauer, R.; Kirchner, C.; Schwegler, V.; Kamp, M.; Leszczynski, M.; Grzegory, I.; Porowski, S. *Phys. Rev. B* **1999**, *60*, 1471–1473.
(18) Christmann, G.; Butté, R.; Feltin, E.; Mouti, A.; Stadelmann, P. A.; Castiglia, A.; Carlin, J.-F.; Grandjean, N. *Phys. Rev. B* **2008**, *77*, 085310.
(19) Özgür, Ü.; Bergmann, M. J.; Casey, H. C.; Everitt, H. O.; Abare, A. C.; Keller, S.; DenBaars, S. P. *App. Phys. Lett.* **2000**, *77*, 109–111.
(20) Malpuech, G.; Carlo, A. D.; Kavokin, A.; Baumberg, J. J.; Zamfirescu, M.; Lugli, P. *App. Phys. Lett.* **2002**, *81*, 412–414.
(21) Lu, T.-C.; Chen, J.-R.; Chen, S.-W.; Kuo, H.-C.; Kuo, C.-C.; Lee, C.-C.; Wang, S.-C. *IEEE J. Sel. Top. Quantum Electron.* **2009**, *15*, 850.
(22) Huang, G.-S.; Lu, T.-C.; Yao, H.-H.; Kuo, H.-C.; Wang, S.-C.; Lin, C.-W.; Chang, L. *Appl. Phys. Lett.* **2006**, *88*, 061904.
(23) Houdré, R.; Weisbuch, C.; Stanley, R. P.; Oesterle, U.; Pellandini, P.; Ilegems, M. *Phys. Rev. Lett.* **1994**, *73*, 2043–2046.
(24) Sellers, I. R.; Semond, F.; Leroux, M.; Massies, J.; Zamfirescu, M.; Stokker-Cheregi, F.; Gurioli, M.; Vinattieri, A.; Colocci, M.; Tahraoui, A.; Khalifa, A. A. *Phys. Rev. B* **2006**, *74*, 193308.
(25) Wang, S.-C.; Lu, T.-C.; Kao, C.-C.; Chu, J.-T.; Huang, G.-S.; Kuo, H.-C.; Chen, S.-W.; Kao, T.-T.; Chen, J.-R.; Lin, L.-F. *Jpn. J. Appl. Phys.* **2007**, *46*, 5397–5407.
(26) Eliseev, P. G.; Perlin, P.; Lee, J.; Osiński, M. *App. Phys. Lett.* **1997**, *71*, 569–571.
(27) Lee, J.-C.; Wu, Y.-F.; Wang, Y.-P.; Nee, T.-E. *J. Cryst. Growth* **2008**, *310*, 5143–5146.
(28) Kavokin, A. V.; Baumberg, J. J.; Malpuech, G.; Laussy, F. P. *Microcavities*; Oxford University Press, Inc.: New York, 2007.
(29) Houdré, R.; Stanley, R. P.; Ilegems, M. *Phys. Rev. A* **1996**, *53*, 2711.
(30) Tawara, T.; Gotoh, H.; Akasaka, T.; Kobayashi, N.; Saitoh, T. *Phys. Rev. Lett.* **2004**, *92*, 256402.
(31) Antoine-Vincent, N.; Natali, F.; Byrne, D.; Vasson, A.; Disseix, P.; Leymarie, J.; Leroux, M.; Semond, F.; Massies, J. *Phys. Rev. B* **2003**, *68*, 153313.
(32) Ollier, N.; Natali, F.; Byrne, D.; Disseix, P.; Mihailovic, M.; Vasson, A.; Leymarie, J.; Semond, F.; Massies, J. *Jpn. J. Appl. Phys.* **2005**, *44*, 4902–4908.
(33) Choi, C. K.; Kwon, Y. H.; Little, B. D.; Gainer, G. H.; Song, J. J.; Chang, Y. C.; Keller, S.; Mishra, U. K.; DenBaars, S. P. *Phys. Rev. B* **2001**, *64*, 245339.
(34) Solnyshkov, D.; Petrolati, E.; Carlo, A. D.; Malpuech, G. *App. Phys. Lett.* **2009**, *94*, 011110.